IOP Publishing Physica Scripta
Phys. Scr. 95 (2020) 045403 (11pp) https://doi.org/10.1088/1402-4896/ab687f

Evolution of plasma parameters in capacitively coupled He–O_2/Ar mixture plasma generated at low pressure using 13.56 MHz generator

Zakia Anjum[1], Maria Younus[2] and N U Rehman[1,3]

[1] Plasma Physics Laboratory, Department of Physics, COMSATS University, Islamabad, Pakistan
[2] Department of Physics, Quaid-i-Azam University, Islamabad, Pakistan

E-mail: najeeb-ur-rehman@comsats.edu.pk

Received 1 August 2019, revised 19 December 2019
Accepted for publication 7 January 2020
Published 18 February 2020

Abstract

Low pressure capacitively coupled He–O_2/Ar mixture plasma is investigated using optical emission spectroscopy and Langmuir probe (LP) techniques and the effects of discharge parameters i.e. radio frequency (RF) power, filling gas pressure and oxygen concentration on electron density (n_e), electron temperature (T_e), excitation temperature (T_{exc}), plasma potential (V_p) and electron energy probability function (EEPF) are monitored. It is noted that n_e increases with increase in RF power and filling gas pressure, while it decreases with increasing O_2 concentration. The LP technique and Boltzmann plot method are employed to determine T_e and T_{exc}. T_e and T_{exc} estimated by both methods shows similar decreasing trend with increasing RF power and filling gas pressure. A sudden increase in n_e and decrease in T_e is noted with RF power, indicating a mode transition i.e. from alpha (α) to the gamma (γ) mode. The threshold RF power for the γ mode shifts from higher to lower value (150–120 W) with increasing gas pressure (0.3–0.5 mbar). This trend reverses and shifts from lower to higher RF value i.e. from 110 W (pure helium) to 150 W (8% O_2) with increase in O_2 concentration. Investigation of EEPF profile states evolution from Druyvesteyn-like to bi-Maxwellian distribution with increase in RF power and filling gas pressure; due to mode transition and decrease in the height of high energy tail of EEPF. Similarly, the effect of O_2 mixing on the shape of EEPF is also investigated. It is noted that in pure helium discharge the EEPF is bi-Maxwellian in nature, while addition of O_2 in the mixture results in the broadening of the EEPF. Moreover, the height of high energy tail of EEPF also increases. Finally, an increasing trend in atomic oxygen density [O] is noted with increase in RF power, pressure and O_2 concentration.

Keywords: CCP, alpha (α) mode, gamma (γ) mode, EEPF, langmuir probe (L.P), Boltzmann plot

(Some figures may appear in colour only in the online journal)

1. Introduction

The radio frequency capacitively coupled plasmas (RF-CCP) have been investigated to great extent due to the wide-range of applications in microelectronics industry e.g. removal and deposition of organic and inorganic materials and surface treatment [1–3]. Low pressure CCP discharges are stable and offer high voltage sheath and ion energies. However, the ion-bombardment energy cannot be controlled independently from the ion flux and low electron densities are reported. Lately, CCP discharges with higher electron density and low ion bombardment energy have been investigated [1, 4, 5].

[3] Author to whom any correspondence should be addressed.

Due to the large area, parallel plate capacitively coupled reactors can also be used for plasma enhanced chemical vapor deposition, in which deposition rate can be enhanced by increasing RF power [6]. Different working gases and their mixtures can be used depending on desired applications.

Capacitively coupled RF helium plasmas are stable and non-equilibrium in nature due to comparatively high electron mobility and heat conductivity which qualifies it to be used for efficient operation, not only at low pressure but also at atmospheric pressure [7–9]. Helium metastable states, acting as energy reservoir, also play a vital role to sustain the plasma through *Penning* ionization, as well as interact with other species and thereby initiating chemical reactions in the plasma itself and also on the surface exposed to it [9]. To achieve more technological benefits, reactive molecular gases like O_2, N_2 and CF_4 are added in small percentages to generate chemically active species [10, 11]. The addition of a few percent of oxygen can provide oxidative power by producing high number densities of reactive oxygen species (ROS) [12–16]. These species include O_2 metastable, O_2 ions or O atoms which act as a reactant for the oxidation of material surface. Moreover, these species are also important for surface modification and deactivation of the bacteria [17, 18]. Oxygen containing plasmas are also found to be effective to improve the properties of biocompatible surfaces [19, 20] and for the removal of photoresist films on the surfaces thus cleaning the substrate after etching process [21, 22].

Several investigations on characterization of He–O_2 mixture plasma at atmospheric pressure have been performed. Kimura *et al* performed electrical and optical measurements of capacitively coupled RF He/O_2 mixture discharge at atmospheric pressure by varying O_2 fraction from 0 to 4% in helium discharge [7]. Jin *et al* explored a fluid model to study the production of ROS in atmospheric pressure RF He/O_2 mixture discharge and found a good agreement between simulation and experimental results [23]. Chen *et al* did numerical study to explore the effect of O_2 concentration on electron energy distribution function (EEDF) in atmospheric He/O_2 and Ar/O_2 plasmas in three different discharge phases using particle-in-cell Monte-Carlo collision model [24]. Zhang *et al* used one-dimensional fluid model to investigate energy efficiencies in producing ROS densities and wall fluxes in He–O_2 dielectric barrier discharges for varying O_2 concentrations [25].

Most of the studies on He–O_2 mixture plasma have been conducted at atmospheric pressure and limited literature is available for capacitively coupled He–O_2/Ar mixture plasma in the low-pressure regime. The low-pressure systems offer benefits over their atmospheric pressure counterparts such as accelerating the electrons to higher energies due to their larger mean free path at low pressure. This effect enables high temperature processes like excitation, ionization and dissociation to occur at relatively lower gas temperatures [26]. Also at low pressure, due to the large mean free path of the electrons, the kinetic effects become more important [27]. In the presence of electronegative gases like O_2, low pressure plasma can offer complex mixture of excited and reactive species, energetic radiations and ions which bombard the target surfaces and initiate quick erosion of biological material and inactivation of bacteria, while remain relatively harmless to underlying substrate [26, 28]. The plasma chemistry can also be affected by the different systems variables like gas pressure, gas flow rate, applied RF power, temperature of the substrate, reactor-configuration and materials of construction which are used for the optimization of the process.

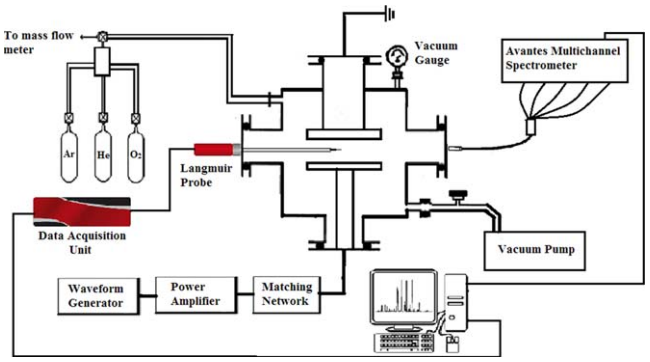

Figure 1. Schematic diagram of experimental setup.

In the present study, He–O_2/Ar mixture plasma at low pressure is characterized to explore optimum conditions for different applications especially for plasma-based sterilization. Plasma parameters like electron density (n_e), electron temperature (T_e) and EEDF are particularly more important for understanding the mechanism governing different processes in the plasma. Thus effect of discharge parameters (RF Power, filling gas pressure and different O_2 concentrations) on electron density (n_e), electron temperature (T_e), excitation temperature (T_{exc}) plasma potential (V_p), evolution of electron energy probability function (EEPF) and atomic oxygen density [O] is explored. To investigate these parameters, single Langmuir probe (LP) and optical emission spectroscopy (OES) techniques are used. To estimate [O], trace rare gas optical emission actinometry technique is employed. Finally, electron temperature measured by LP and excitation temperature measured by Boltzmann plot method has been compared.

2. Material and methods

Figure 1 shows the schematic illustration of experimental setup. An arbitrary waveform signal generator TGA12104 and PRANA broadband power amplifier (DP 140 DC) coupled with a matching network were used to feed RF power to a capacitively coupled plasma source, at an operating frequency of 13.56 MHz. He–O_2/Ar plasma was generated and sustained in an indigenously developed stainless steel chamber of height 42 cm and diameter 39 cm. The diameter of the electrodes was 14 cm and the separation between them was 4.5 cm. Before filling the gases, the chamber was evacuated using rotary vane pump to a base pressure of 0.003 mbar. The gases flow rates were monitored and controlled using Teledyne Hastings mass flow meters. Data was acquired at a fixed flow rate of 25 SCCM for pure He and He–O_2/Ar mixture

discharge. The He/O_2 concentrations were varied, while the Ar fraction, being used as an actinometer, was kept fixed at 4%. O_2 concentration was increased while He concentration was decreased for each set of data till the maximum O_2 concentration was 24%. The filling gas pressure was varied from 0.3 to 0.5 mbar, while RF power was varied from 20 to 160 W. The time-integrated emission spectra were recorded by an AVANTES (five-furcated) high-resolution spectrometer, having resolution 0.06–1.3 nm (at FWHM) and spectral range 250–900 nm. These spectra were then normalized for the spectral response of the optical fiber, grating and optical window. OES technique was used to estimate the excitation temperature (T_{exc}) and atomic oxygen density [O] by analyzing these normalized spectra while a single RF compensated LP, purchased from Impedans Ltd was used to estimate the electron density (n_e), electron temperature (T_e), plasma potential (V_p), and EEPF.

2.1. LP measurements

The LP used in the study is a single RF compensated LP (Impedans Ltd), consisting of a single wire made up of tungsten whose length and radius are 10 mm and 0.195 mm respectively. Only 5 mm of the probe tip is exposed to the plasma while the remaining 5 mm is covered with ceramic tube. The probe is placed between two electrodes to characterize the bulk plasma by measuring current drawn from plasma to the probe as a function of voltage relative to a reference surface. The upper electrode and the chamber wall are grounded and serve as the reference surface for LP measurements. The probe current is collected by applying bias voltages in the range of −20 to 50 V with the voltage step size of 0.5 V. To avoid contaminations, the probe tip cleaning feature is used by applying 150 V biasing voltage to clean the probe between the scans through electron bombardment. The Automated Langmuir Probe Software, provided by Impedans Ltd analyzed the *I–V* characteristic curves to measure electron density (n_e), electron temperature (T_e), plasma potential (V_p), and EEPF.

Plasma potential (V_p), the potential on the *I–V* characteristics at the transition point between electron retarding and electron saturation region, is determined by the intersecting slope method whereas electron temperature (T_e) and electron density (n_e) are calculated from *I–V* characteristics curves of LP using current measured at V_p as;

$$\frac{1}{kT_e} = \frac{I(V_p)}{\int_{V_f}^{V_p} I(V)\mathrm{d}V} \tag{1}$$

and

$$n_e = \frac{I(V_p)}{A_p}\sqrt{\frac{2\pi m_e}{e^2 k_B T_e}}, \tag{2}$$

where equations (1) and (2) are valid for Maxwellian distribution. In these equations, k_B is the Boltzmann constant, $V_p$and V_f are the plasma potential and the floating potential, respectively, V is the probe bias with respect to the plasma potential and I is the probe current. In equation (2), A_p is the probe area, m_e is the mass of electron and e is the charge of electron.

The EEDF of the plasma is estimated from the second derivative of the *I–V* characteristics, with ion current subtracted from the total probe current, by applying the 'Druyvesteyn Method' as [29, 30]:

$$\frac{\mathrm{d}^2 I_e}{\mathrm{d}V^2} = \frac{e^2 A_p}{4}\sqrt{\frac{2e}{mV}} f_e(\varepsilon). \tag{3}$$

Here $f_e(\varepsilon)$ is the EEDF, ε is the energy variable, I_e is the electron retarding current, V is the probe bias with respect to plasma potential V_p, A_p is the surface area of the probe tip, e and m_e are the charge and mass of electron respectively. Usually, it is convenient to express the electron distribution in terms of EEPF denoted by $F(\varepsilon)$, rather than EEDF; as it is more helpful in determining the nature of the distribution. The EEPF $F(\varepsilon)$ can be related to EEDF as;

$$F(\varepsilon) = \varepsilon^{-1/2} f_e(\varepsilon). \tag{4}$$

2.2. OES measurements

OES is a non-intrusive and reliable technique used to estimate the plasma parameters. Currently, excitation temperature (T_{exc}) is estimated using Boltzmann plot method, while trace rare gas optical emission actinometry technique is used to determine atomic oxygen density [O] in $He–O_2/Ar$ mixture plasma.

2.2.1. Excitation temperature. The electron temperature (T_e) is a key parameter which plays active role in the generation of reactive species. Different reaction rates like electron impact excitation, dissociation, and ionization etc are strongly affected by variation in T_e. It also controls the chemical reactions occurring inside the plasma. Besides intrusive LP technique, T_e can also be determined by OES based on equilibrium models. However, determination of T_e directly from spectral lines is not always straightforward due to cumbersome interpretation using complex equilibrium models. The excitation temperature (T_{exc}), on the other hand, is sometimes more proficient to characterize the plasma. The reason for this is that T_{exc}, which governs the population of excited levels, is comparatively easy to determine [31]. Moreover, when the electron density is greater than a critical value established by the Griem criterion, the system is in local thermodynamic equilibrium (LTE) and in this case T_{exc} is close to T_e [32]. The laboratory or industrial processing low pressure plasma rarely satisfies LTE condition and thus T_{exc} is different from T_e in such non-equilibrium plasma. However, T_{exc} can still give the estimation of the electron temperature, when excited levels populate according to Boltzmann distribution, and follow the similar trend with respect to different discharge parameters and thus can be a good alternate diagnostic in different discharges [31].

The present study deals coronal equilibrium in which electron impact excitation is the forward process and spontaneous decay is the reverse process and Boltzmann plot

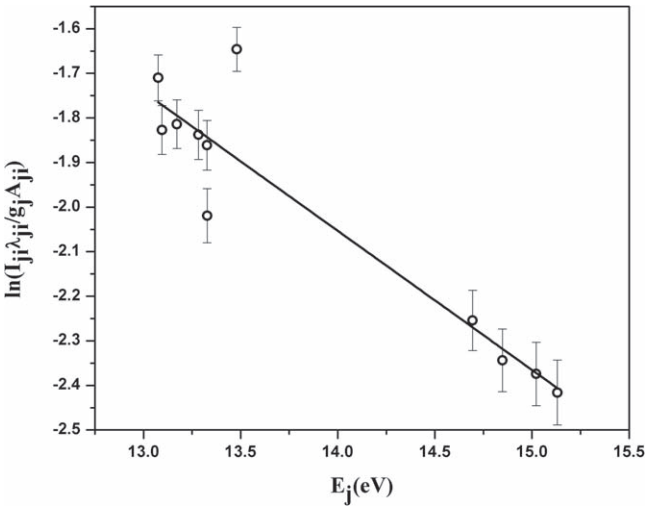

Figure 2. Boltzmann plot used to estimate T_{exc} in He 92%-O_2 4%-Ar 4% gas mixture for 0.3 mbar pressure and 150 W RF power.

technique gives excitation temperature T_{exc} rather than electron temperature [33]. To obtain T_{exc}, Ar I emission lines are used by assuming that upper energy levels of these lines populate following Boltzmann distribution. Under this condition, atomic emission intensity (I_{ji}) of the transition from level j to level i is given by [34];

$$I_{ji} = \frac{hc}{\lambda_{ji}} \frac{n g_j A_{ji}}{Z(T_{exc})} \exp\left(-\frac{E_j}{k_B T_{exc}}\right), \tag{5}$$

where h is the Planck constant, c is the speed of light, λ_{ji} is the wavelength of the corresponding transition, n is the total population of particular species in all atomic states, g_j is the statistical weight of level j, A_{ji} is the transition probability of spontaneous emission between the levels j and i, also called the Einstein coefficient, $Z(T_{exc})$ is the partition function, E_j is the energy of the upper level j, k_B is the Boltzmann constant and T_{exc} is the excitation temperature. Rearranging equation (5), we get

$$\ln\left(\frac{I_{ji}\lambda_{ji}}{g_j A_{ji}}\right) = -\frac{E_j}{k_B T_{exc}} + \text{constant}. \tag{6}$$

This is equation of straight line and from inverse of the slope of above Boltzmann plot T_{exc} can be estimated. Figure 2 shows the Boltzmann plot of the experimental data obtained at 0.3 mbar and 150 W with 4% O_2 concentration in the mixture. The spectroscopic data corresponding to the lines selected for this study is given in table 1.

2.2.2. Measurement of the ground state atomic oxygen density using actinometry. Actinometry is a popular OES based technique used for qualitative and sometimes quantitative determination of particle densities in a discharge. This method was first introduced by Coburn and Chen [36] in which a small amount (1%–5%) of a noble gas (e.g. Ar) is added as an actinometer whose ground state atomic density is known. Comparative measurement of the emission line intensities of

Table 1. Spectroscopic data corresponding to selected Ar lines for the calculation of T_{exc} [35].

λ_{ji} (nm)	E_j (eV)	g_j	$A_{ji}(10^8 s^{-1})$	Spectral response R
603.21	15.13	9	0.0246	0.34
693.76	14.69	1	0.0308	0.39
696.5	13.33	3	0.064	0.37
720.69	15.02	3	0.0248	0.30
731.17	14.84	3	0.0170	0.28
750.4	13.48	1	0.45	0.28
794.8	13.28	3	0.186	0.19
800.6	13.17	5	0.049	0.18
811.5	13.07	7	0.33	0.14
826.5	13.33	3	0.153	0.12
842.5	13.10	5	0.215	0.11

the actinometer and the species of unknown density leads to a simple relation:

$$\frac{[Y]}{[Act]} = c\frac{I_Y}{I_{Act}}. \tag{7}$$

Here $[Y]$ is the unknown atomic density of species Y and $[Act]$ is the known atomic density of the actinometer. I_Y and I_{Act} are the optical emission line intensities of the species of interest Y and the actinometer respectively. The factor C is considered to be a constant. The basic requirements for an actinometry relation (equation (7)) used to measure the unknown density of reactive species are as follows:

(i) Electron impact excitation directly from the ground state is the main excitation mechanism for both the actinometer and the species of interest.
(ii) Electron impact excitation cross-sections for the actinometer and the species of interest have similar threshold energies and energy dependencies.
(iii) Quenching processes are insignificant.

In He–O_2 mixture plasma, Ar is added in a small amount, as an actinometer, to determine the atomic oxygen density $[O]$. Two spectral lines Ar ($2p_1$–$1s_2$) at 750 nm and O (^{3}P–^{3}S) at 844 nm are selected for actinometric measurements. Following excitation and de-excitation channels for the selected spectral lines are used [37].

Ar ($2p_1$) state is populated mainly through electron impact excitation from the ground state, as the basic requirement for actinometry to be valid, while two step excitations can be neglected;

$$e + \mathrm{Ar}(1p_0) \xrightarrow{k_{\mathrm{Ar}}^{2p_1}} \mathrm{Ar}(2p_1) + e. \tag{8}$$

The oxygen excited state O ($3p\ ^3P$), on the other hand, can be populated by two mechanisms:

i) Direct electron impact from ground state;

$$e + \mathrm{O}(2p^4\ ^3P) \xrightarrow{k_{\mathrm{O}}^{3p}} \mathrm{O}(3p\ ^3P) + e. \tag{9}$$

ii) Dissociative excitation of ground state molecule by electronic collision;

$$e + O_2 \xrightarrow{k_{dis}^{3p}} O + O(3p\ ^3P) + e. \quad (10)$$

The excited states are depopulated through radiative de-excitation as

$$Ar(2p_1) \xrightarrow{A_{ji}^{2p_1}} Ar(1p_0) + h\upsilon(750.4\ nm) \quad (11)$$

$$O(3p\ ^3P) \xrightarrow{A_{ji}^{3p}} O(3s\ ^3S) + h\upsilon(844.6\ nm). \quad (12)$$

The quenching of O ($3p\ ^3P$) state by O_2 molecule is considered negligible as pressure is low. Considering equations (8)–(12) as production and destruction mechanisms for the given excited states, the theoretical emission intensities of the selected Ar and O lines can be written as;

$$I_{750} = \frac{n_e h\upsilon_{750} A_{ji}^{2p_1} k_{Ar}^{2p_1}[Ar]}{\sum A_{ji}^{2p_1}} \quad (13)$$

$$I_{844} = \frac{n_e h\upsilon_{844} A_{ji}^{3p} (k_O^{3p}[O] + k_{dis}^{3p}[O_2])}{\sum A_{ji}^{3p}} \quad (14)$$

here n_e is the density of electrons and $\sum A_{ji}$ is the cumulative transition probability from level j to lower level i. $k_{Ar}^{2p_1}$ and k_O^{3p} are the rate coefficients of direct electron impact excitation from ground state of Ar and O_2 respectively while k_{dis}^{3p} is the dissociative excitation rate coefficient of O_2 molecule. These rate coefficients are measured through Bolsig$^+$ (Siglo Kinema); Boltzmann equation solver by assuming Maxwellian EEDF [38]. The cross sections used to calculate these rate coefficients for the selected argon Ar ($2p_1$) 750 nm and oxygen O (^{3}P) 844 nm lines are taken from the literature [37, 39].

Taking the ratio of oxygen line intensity I_{844} to the argon line intensity I_{750};

$$\frac{I_{844}}{I_{750}} = \frac{h\upsilon_{844} A_{ji}^{3p}}{h\upsilon_{750} A_{ji}^{2p_1}} \frac{\sum A_{ji}^{2p_1}}{\sum A_{ji}^{3p}} \frac{(k_O^{3p}[O] + k_{dis}^{3p}[O_2])}{k_{Ar}^{2p_1}[Ar]}. \quad (15)$$

Simplifying and rearranging the equation;

$$[O] = C_{3p}^{2p_1} \frac{I_{844}}{I_{750}} \frac{k_{Ar}^{2p_1}}{k_O^{3p}}[Ar] - \frac{k_{dis}^{3p}}{k_O^{3p}}[O_2], \quad (16)$$

where $C_{3p}^{2p_1} = \frac{h\upsilon_{750} A_{ji}^{2p_1}}{h\upsilon_{844} A_{ji}^{3p}} \frac{\sum A_{ji}^{3p}}{\sum A_{ji}^{2p_1}}$ is a constant.

The contribution of dissociative excitation in the production of oxygen excited state O (3p ^{3}P) is small i.e. $\frac{k_{dis}^{3p}}{k_O^{3p}} \ll 1$ as shown in figure 3 and thus can be neglected. The density ratio is then given by;

$$\frac{[O]}{[Ar]} = C_{3p}^{2p_1} \frac{I_{844}}{I_{750}} \frac{k_{Ar}^{2p_1}}{k_O^{3p}} = 1.12 \frac{I_{844}}{I_{750}} \frac{k_{Ar}^{2p_1}}{k_O^{3p}}. \quad (17)$$

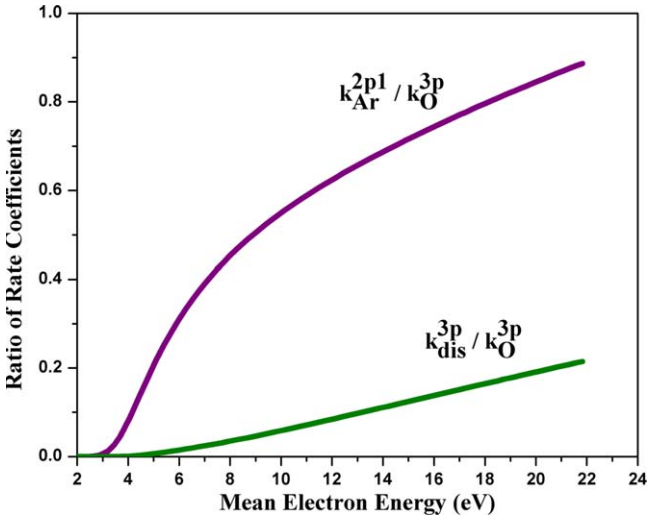

Figure 3. Variation of the ratio of rate coefficients $k_{Ar}^{2p_1}/k_O^{3p}$ and k_{dis}^{3p}/k_O^{3p} as function of mean electron energy.

3. Results and discussion

Electron density (n_e) and electron temperature (T_e) are the key parameters which control the production and destruction rates of active species generated in the plasma. Currently, these two parameters and EEPF are studied using OES and LP techniques. Figures 4(a) and (b) show the variation in n_e measured with LP as a function of applied RF power, filling gas pressure and different gases concentration. It is clear from the figure 4(a) that n_e increases with RF power and filling gas pressure at 4% O_2 concentration in the mixture. This behavior of n_e is due to energy gained by the electrons, as the RF power increases, which become energetic enough to cause enhanced ionization and excitation, resulting in an increase in n_e. Whereas increased n_e at higher filling gas pressure is due to decrease in mean free path. Similarly, higher concentration of He in the mixture is also responsible for the increase in n_e due to *Penning* ionization ($He^m + O_2 \rightarrow He + O_2^+ + e$) with increasing pressure [11, 40]. Moreover, at higher RF power, an abrupt increase in n_e is also observed which indicates mode transition from the alpha (α) to the gamma (γ) mode. It is clear from figure that mode transition initiates at 150 W for 0.3 mbar pressure and it shifts towards lower power i.e. 130–120 W with increase in pressure from 0.4 to 0.5 mbar respectively. Figure 4(b) shows the variation in n_e with RF power for pure He and different O_2 concentrations in the mixture. It is noted that n_e exhibits similar trend for RF power in pure He as well as for two different O_2 concentrations but decreasing trend in n_e is noted with increase in O_2 concentration in the mixture. This fact can be explained as; at higher O_2 concentration the *Penning* ionization process reduces, resulting in a decreasing trend of n_e. Moreover, due to the electronegative nature of oxygen, O^- and O_2^- are formed relatively easy through the electron impact dissociation ($O_2 + e^- \rightarrow O + O^-$) and three body attachment ($e^- + O_2 + M \rightarrow O_2^- + M$) of electrons to O_2 molecules [41, 42], which leads to a decrease in n_e. RF power required for operating the discharge in γ mode is also shifted towards

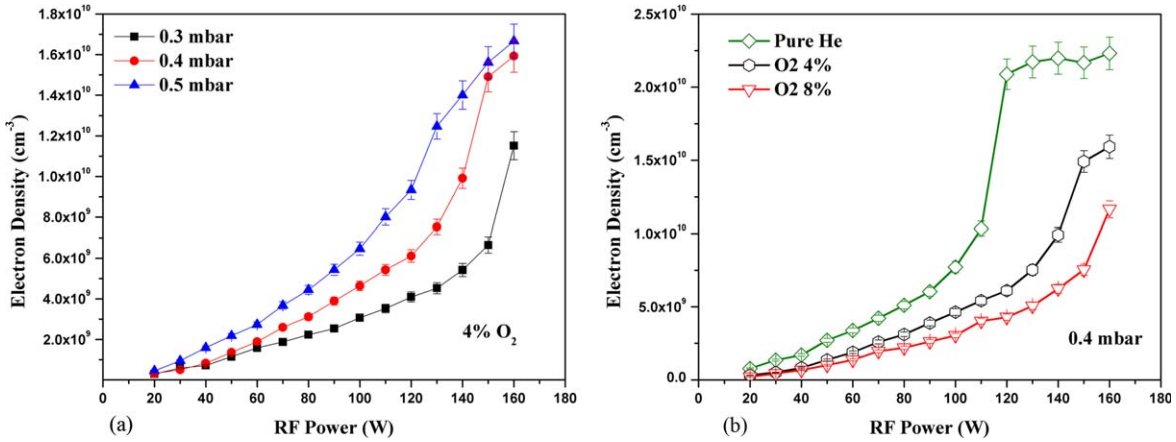

Figure 4. Variation in electron density n_e with RF power and (a) filling gas pressure with 4% O_2 in the mixture (b) different O_2 concentration at 0.4 mbar pressure.

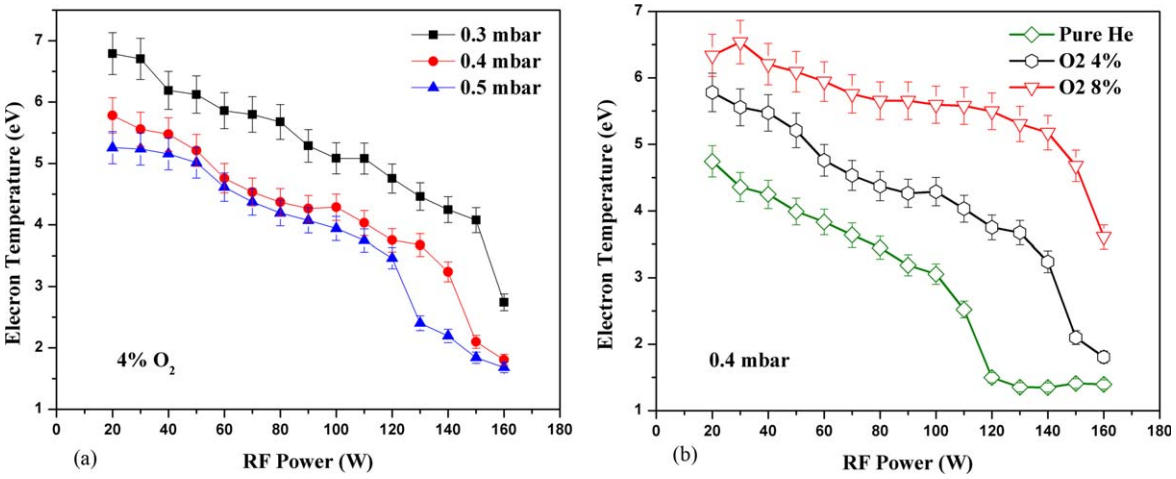

Figure 5. Variation in electron temperature T_e with RF power and (a) filling gas pressure with 4% O_2 in the mixture (b) different O_2 concentration at 0.4 mbar pressure.

higher values i.e. from 110 W, for pure He discharge, to 140 W and 150 W with the addition of 4% and 8% O_2 in the mixture, respectively. This shifting of RF power towards higher values can be attributed to the increase in energy loss through molecular rotational and vibrational excitations along with dissociative processes associated with the addition of O_2 in the mixture. Since, these processes do not directly contribute to ionization processes and, therefore higher RF powers are required for the discharge to operate in γ mode [9].

Figure 5 represents the variation of T_e (measured by LP) with RF power, filling gas pressure and different gases concentration. It is clear in figure 5(a) that T_e exhibits the decreasing trend with both RF power and filling gas pressure at a fixed O_2 concentration. This decreasing trend with RF power is due to the increase in n_e, leading to increase in electron–electron collision frequency compared to electron–neutral collision and resulting in the decrease in T_e. Similarly decrease in T_e is also due to increase in collision frequency with the increase in pressure. Moreover, a sudden decrease in T_e is also noted at 150 W, 130 W and 120 W for the pressures of 0.3 mbar, 0.4 mbar and 0.5 mbar, respectively. This abrupt decrease is attributed to a transition of the discharge from the α to the γ mode due to an abrupt increase in n_e at these powers, as shown in figure 4(a). On the other hand, figure 5(b) depicts the variation in T_e with RF power for pure He and two different O_2 concentrations, at a fixed pressure of 0.4 mbar. It is noted that T_e decreases with RF power for pure He and different O_2 concentrations but it increases with increasing O_2 concentration in the mixture. This trend can be related to decrease in n_e due to electron attachment processes with increasing O_2 concentration in the mixture. This results in the decrease in electron–electron collision frequency, thereby giving the electrons enough time to gain energy between successive collisions and thus increasing T_e.

Figure 6 shows the comparison of $T_e(LP)$ measured by the LP and $T_{exc}(OES)$ measured by the Boltzmann plot method; as a function of RF power and filling gas pressure at a fixed O_2 concentration. It is clear from the figure that both $T_e(LP)$ and $T_{exc}(OES)$ exhibit similar decreasing trend with RF power and gas pressure. Since in non-thermal plasma the Boltzmann plot method, based on OES, gives T_{exc} while LP provides T_e thus higher value of $T_e(LP)$ is noted compared to $T_{exc}(OES)$. In addition, minor deviation in the 2nd derivative

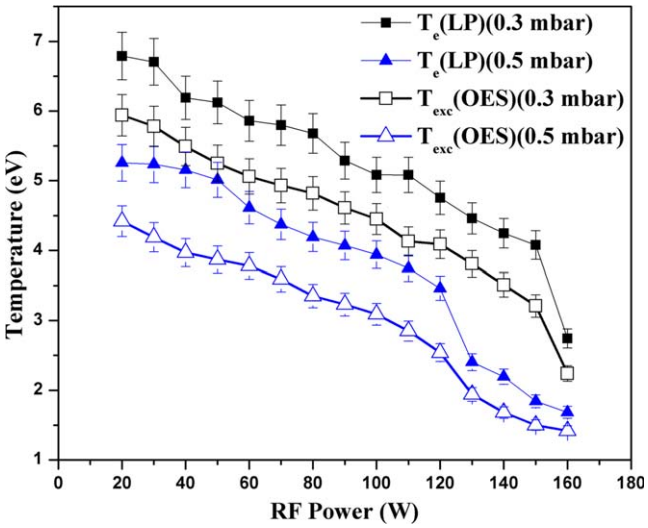

Figure 6. Variation in $T_e(LP)$ and $T_{exc}(OES)$ with RF power and filling gas pressure with 4% O_2 in the mixture.

of *I–V* characteristics from the usual course is noted due to insufficient RF compensation at low RF powers, leading to higher value of T_e determined by LP.

Plasma potential (V_p) is another significant parameter which regulates the ion energy in the sheath region. Any variation in it controls the strength of the electric field that energizes the electrons and gives rise to ionization processes to sustain the discharge. Figure 7(a) shows the variation in V_p with RF power at two filling gas pressure and with 4% O_2 concentration in the mixture. It is clear from figure that V_p increases with the increase in RF power. However, at low RF powers i.e. up to 80 W, rapid increase in V_p is noted which may be due to smaller degree of ionization at low RF powers and due to diffusion of electrons towards the wall. This increasing trend persisted but the rate of increase is comparatively low and become nearly steady at 140 W. Although n_e continuously increases at higher RF power, some electrons might be consumed by the oxygen atoms and molecules to form negative ions, thus causing continuous increase in V_p. On the other hand, slight decrease in V_p is observed with the increase in pressure due to the increase in n_e with pressure. Similarly, variation in V_p with different O_2 concentration in the mixture is shown in figure 7(b) and slight difference in the V_p for two different O_2 concentrations is noted up to 70 W RF power. But at higher RF powers V_p increases for higher O_2 concentration due to decrease in n_e (figure 4(b)).

To understand the kinetics of the discharge, the evolution in EEDF has also been discussed because, in non-thermal plasma, it defines the heating mechanism and various collision processes in the discharge [24]. It is therefore important to have a profound knowledge about the electron energy and its distribution in the plasma. For better understanding, it is customary to show the energy distribution function in terms of EEPF. Figure 8(a) shows the evolution in EEPF, measured with LP, with RF power at 0.4 mbar pressure and 4% O_2 in the mixture. It is clear from the graph that with increase in RF power i.e. 20–160 W, a significant increase in the density of bulk electrons (0–5 eV) is noted. Moreover, it is also noted that at low RF powers, EEPF are convex and have Druyvesteyn-like shape while with increase in RF power, beyond 100 W, EEPF width decreases and it evolve from Druyvesteyn to bi-Maxwellian. As a result, T_e decreases which is evident in figure 5. These facts can be explained as; at low RF power collisional or ohmic heating is responsible for sustainment of the discharge and thus broadening in EEPF profile is observed [43]. RF field (E), responsible for collisional heating, is inversely proportional to the n_e i.e. $E \propto J_O / n_e$, where J_O is the discharge current density. Thus a lower n_e, at low RF power, leads to an higher RF electric field within the plasma bulk which is responsible for enhancing the broadening due to collisional heating [44]. On the other hand, at higher RF power beyond 100 W, the EEPF becoming concave, narrow and shape resembles to bi-Maxwellian. This change in shape between 130 and 160 W indicating the initiation of mode transition, i.e. from the alpha (α) to the gamma (γ) mode, at a given pressure and O_2 concentration [45]. This happens when large amount of applied RF power is consumed in the sheath region to accelerate the ions. These accelerated ions collide with the surface of electrodes and cause secondary electron emission. Moreover, in the γ mode ionization predominantly occurs by secondary electrons and consequently, electron temperature decreases as depicted in figure 5. Further, dips in EEPF profiles beyond 20 W are noted, in the energy range of 7–10 eV, which might be due to loss of electrons through inelastic collisional process such as vibrational or rotational excitation of O_2 molecule.

Figure 8(b) shows the evolution in EEPF with pressure at 150 W RF power and 8% O_2 in the mixture. It is clear from the graph that EEPF transforms from Druyvesteyn-like to bi-Maxwellian due to conversion of the shape of EEPF from convex to concave; as pressure changes from 0.3 to 0.5 mbar and increase in electron density is noted. Moreover, height of high energy tail of EEPF decreases with the increasing gas pressure. This decrease in height of high energy tail of EEPF indicates the decrease in density of high energy electrons; whose energies are closer to ionization potential (I.P) of O_2 ($\approx$12 eV). This variation is consistent with the relation for ionization rate constant with neutral gas density as [1];

$$\frac{k_{ion}}{v_B} = \frac{1}{n_g d_{eff}}, \tag{18}$$

where k_{ion} is the ionization rate constant evaluated by using normalized EEDF, v_B is the Bohm velocity, n_g is the neutral gas density and d_{eff} is the effective plasma size. The dependency of k_{ion} on EEDF or T_e is greater as compared to the dependency of v_B, thus the ionizing tail of EEPF decreases with the increase in pressure in accordance with the reduction in the ionization rate constant due to the higher density of n_g with increasing pressure [43].

The effect of O_2 mixing on the evolution in EEPF at fixed RF power of 150 W and 0.4 mbar pressure is shown in figure 8(c). It is clear from the figure that for pure He discharge EEPF is bi-Maxwellian in nature and higher electron density is noted because, for the given pressure and RF power, discharge operates in the γ mode; as shown in figure 4(b). Moreover, broadening in EEPF is noted with

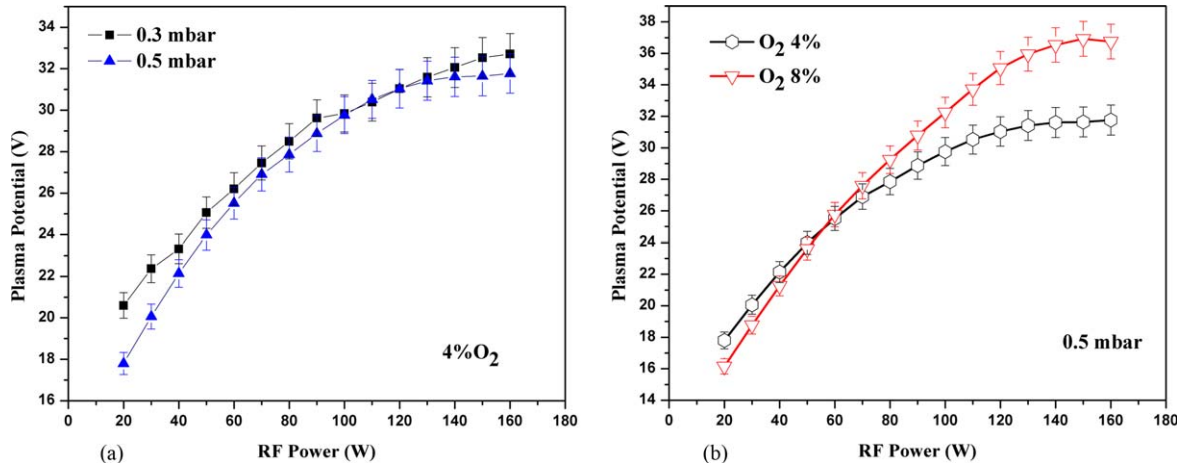

Figure 7. Variation in plasma potential V_p with RF power and (a) filling gas pressure with 4% O_2 in the mixture (b) different O_2 concentration at 0.5 mbar pressure.

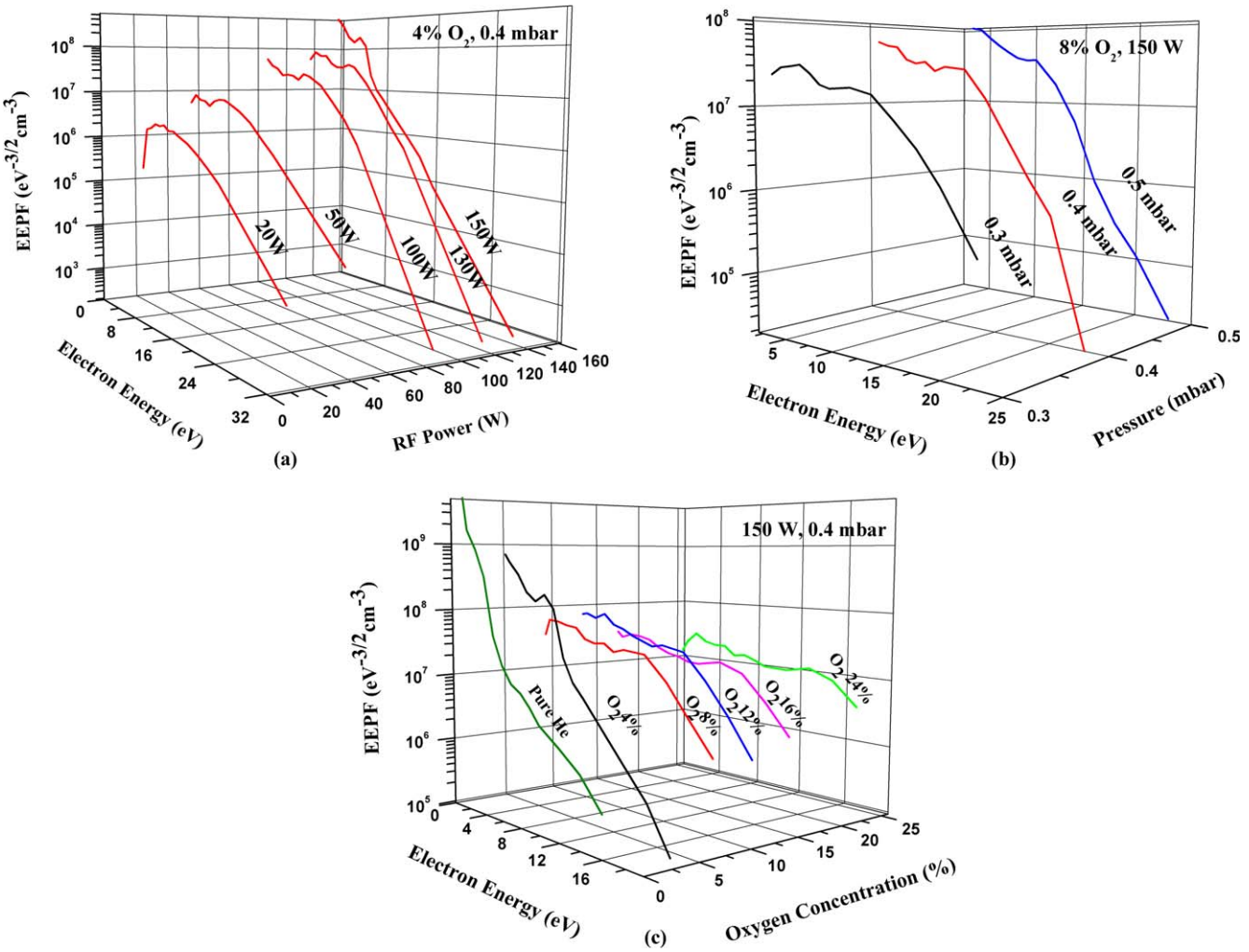

Figure 8. Evolution of EEPF (a) with RF power at 0.4 mbar pressure and 4% O_2 concentration in the mixture (b) with various pressures at 150 W RF power and 8% O_2 concentration in the mixture (c) at pure He and different O_2 concentrations in the mixture at 150 W RF power and 0.4 mbar filling gas pressure.

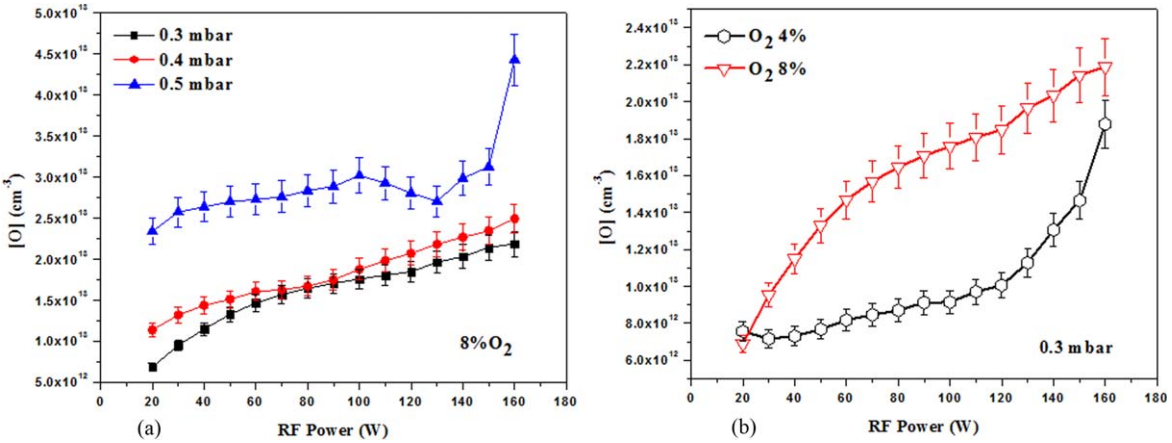

Figure 9. Variation in atomic oxygen density $[O]$ with RF power and (a) filling gas pressure with 8%O_2 in the mixture (b) different O_2 concentration at 0.3 mbar pressure.

increase in O_2 concentration in the mixture. This broadening effect is attributed to collisional heating of bulk plasma; due to shifting of discharge from the γ to the α mode; with increase in O_2 concentration in the mixture. Since the collisional heating occurs due to momentum transfer mechanism, which randomizes the direction of electron momentum and allows the kinetic energy to be gained from RF electric field within bulk plasma [44], therefore higher electron temperatures are noted at higher O_2 concentrations (figure 5(b)). Moreover, it is worth noting that the broadening in EEPF increases with increase in O_2 concentration and dip around ≈12 eV (I.P of O_2) shifts towards higher energy (≈14 eV); when O_2 concentration varies from 4% to 24% in the mixture. This indicates the increase in inelastic collisional process such as vibrational or rotational excitation of O_2 molecule. Similarly, height of high energy tail of EEPF increases with increase in O_2 concentration. This may be the result of superelastic collisions which occur due to presence of high density of electronic metastable states in the discharge. These superelastic collisions are known to produce additional peaks as well as to enhance the ionizing tail of EEPF [44, 46, 47].

Atomic oxygen is an important product among ROS produced in electrical discharges of oxygen and its mixtures. Figure 9(a) shows the variation in atomic oxygen density $[O]$ with RF power and gas pressure with 8% O_2 in the mixture. It is noted that $[O]$ tends to increase with RF power and filling gas pressure. This tendency of $[O]$ can be justifies with the trend of electron density (n_e). As shown earlier in the figure 4(a) n_e increases with RF power and filling gas pressure which increases the dissociation of O_2 by electron impact, resulting in an increasing trend of $[O]$. The effect of increase in O_2 concentration in the mixture is shown in figure 9(b), where $[O]$ is plotted against RF power at two different O_2 concentrations in the mixture. It is evident from the figure that $[O]$ increases with the increase in O_2 concentration in the mixture as O_2 molecules are needed at the first place for the generation of ground state oxygen atoms. Moreover, with the increase in O_2 concentration, T_e also increases, enabling higher dissociation rates due to higher electron energies, which may also result in the increase in $[O]$.

4. Conclusions

In the present work, the behavior of plasma parameters like electron density (n_e), electron temperature (T_e), excitation temperature (T_{exc}), plasma potential (V_p) and EEPF is studied in low pressure capacitively coupled He–O_2/Ar mixture plasma. The electron density (n_e) is found to increase with increasing power and filling gas pressure but it decreases with increase in O_2 concentration in the mixture. On the other hand, the electron temperature (T_e) shows a decreasing trend with increasing power and filling gas pressure, while it increases with the increasing O_2 concentration. An abrupt increase in n_e and decrease in T_e is also noted due to mode transition from the α to the γ mode. The threshold RF power for initiating the γ mode tends to shift towards lower values with increasing pressure but shifts towards higher values with increasing O_2 concentration in the mixture. The excitation temperature (T_{exc}), measured by the Boltzmann plot method, also shows the similar decreasing trend with RF power and filling gas pressure but has lower values than T_e measured by the LP. The plasma potential (V_p) shows increasing trend with increasing RF power and O_2 concentration in the mixture, but a slight decrease in the values with increase in filling gas pressure is observed. The evolution of EEPF with RF power, filling gas pressure and different O_2 concentrations is also studied. The EEPF evolve from Druyvesteyn-like to bi-Maxwellian distribution and decrease in high energy tail is noted with the increase in RF power and filling gas pressure. The addition of O_2 in the mixture results in an increase in broadening of the EEPF profile along with the appearance of additional peaks and increase in the high energy tail. Atomic oxygen density [O] exhibits an increasing trend with RF power, filling gas pressure and O_2 concentration.

Acknowledgments

The authors acknowledge Higher Education Commission (HEC), Islamabad, Pakistan for full financial support of the

work under the Research Project No. 2997/R&D/14 and TDF-137.

ORCID iDs

N U Rehman https://orcid.org/0000-0001-6062-5836

References

[1] Lieberman M A and Lichtenberg A J 2005 *Principles of Plasma Discharges and Materials Processing* vol 2 (New Jersey: John Wiley & Sons)

[2] May G S and Sze S M 2004 *Fundamentals of Semiconductor Fabrication* (New York: Wiley)

[3] Tanarro I, Herrero V J, Carrasco E and Jiménez-Redondo M 2011 Cold plasma chemistry and diagnostics *Vacuum* **85** 1120–4

[4] Zhu X-M, Chen W-C, Zhang S, Guo Z-G, Hu D-W and Pu Y-K 2007 Electron density and ion energy dependence on driving frequency in capacitively coupled argon plasmas *J. Phys. D: Appl. Phys.* **40** 7019

[5] Raizer Y P, Shneider M N and Yatsenko N A 2017 *Radio-Frequency Capacitive Discharges* (Boca Raton, FL: CRC Press)

[6] Diomede P and Economou D J 2014 Kinetic simulation of capacitively coupled plasmas driven by trapezoidal asymmetric voltage pulses *J. Appl. Phys.* **115** 233302

[7] Kimura T and Hanai T 2006 Experimental study of capacitive He/O_2 discharges at atmospheric pressure *Japan. J. Appl. Phys.* **45** 4219

[8] Sousa J S, Niemi K, Cox L, Algwari Q T, Gans T and O'connell D 2011 Cold atmospheric pressure plasma jets as sources of singlet delta oxygen for biomedical applications *J. Appl. Phys.* **109** 123302

[9] Niemi K, Waskoenig J, Sadeghi N, Gans T and O'Connell D 2011 The role of helium metastable states in radio-frequency helium-oxygen atmospheric pressure plasma jets: measurement and numerical simulation *APS Meeting Abstracts*

[10] Flores O, Castillo F, Martinez H, Villa M, Villalobos S and Reyes P 2014 Characterization of direct current He-N_2 mixture plasma using optical emission spectroscopy and mass spectrometry *Phys. Plasmas* **21** 053502

[11] Younus M, Rehman N, Shafiq M, Zakaullah M and Abrar M 2016 Evolution of plasma parameters in a He-N_2/Ar magnetic pole enhanced inductive plasma source *Phys. Plasmas* **23** 023512

[12] Laroussi M 2005 Low temperature plasma-based sterilization: overview and state-of-the-art *Plasma Process. Polym.* **2** 391–400

[13] Liu D X, Rong M Z, Wang X H, Iza F, Kong M G and Bruggeman P 2010 Main species and physicochemical processes in cold atmospheric-pressure He + O_2 Plasmas *Plasma Process. Polym.* **7** 846–65

[14] Niemi K, Schulz-Von Der Gathen V and Döbele H 2005 Absolute atomic oxygen density measurements by two-photon absorption laser-induced fluorescence spectroscopy in an RF-excited atmospheric pressure plasma jet *Plasma Sources Sci. Technol.* **14** 375

[15] Knake N, Reuter S, Niemi K, Schulz-Von Der Gathen V and Winter J 2008 Absolute atomic oxygen density distributions in the effluent of a microscale atmospheric pressure plasma jet *J. Phys. D: Appl. Phys.* **41** 194006

[16] Ellerweg D, Benedikt J, von Keudell A, Knake N and Schulz-von der Gathen V 2010 Characterization of the effluent of a He/O_2 microscale atmospheric pressure plasma jet by quantitative molecular beam mass spectrometry *New J. Phys.* **12** 013021

[17] Goree J, Liu B and Drake D 2006 Gas flow dependence for plasma-needle disinfection of S. mutans bacteria *J. Phys. D: Appl. Phys.* **39** 3479

[18] Perni S, Shama G, Hobman J, Lund P, Kershaw C, Hidalgo-Arroyo G, Penn C, Deng X T, Walsh J L and Kong M G 2007 Probing bactericidal mechanisms induced by cold atmospheric plasmas with Escherichia coli mutants *Appl. Phys. Lett.* **90** 073902

[19] Jazbec K, Šala M, Mozetič M, Vesel A and Gorjanc M 2015 Functionalization of cellulose fibres with oxygen plasma and ZnO nanoparticles for achieving UV protective properties *J. Nanomater.* **16** 25

[20] Ko Y-M, Myung S-W and Kim B-H 2015 O_2/Ar plasma treatment for enhancing the biocompatibility of hydroxyapatite nanopowder and polycaprolactone composite film *J. Nanosci. Nanotechnol.* **15** 6048–52

[21] Joubert O, Pelletier J and Arnal Y 1989 The etching of polymers in oxygen-based plasmas: a parametric study *J. Appl. Phys.* **65** 5096–100

[22] Collart E, Baggerman J and Visser R 1995 On the role of atomic oxygen in the etching of organic polymers in a radio-frequency oxygen discharge *J. Appl. Phys.* **78** 47–54

[23] He J and Zhang Y 2013 Generation of reactive oxygen species in helium–oxygen radio-frequency discharges at atmospheric pressure *IEEE Trans. Plasma Sci.* **41** 2979–86

[24] Chen X, Tan Z, Liu Y, Wang X and Li X 2018 Effects of oxygen concentration on the electron energy distribution functions in atmospheric pressure helium/oxygen and argon/oxygen needle-electrode plasmas *J. Phys. D: Appl. Phys.* **51** 375202

[25] Zhang H, Guo Y, Liu D, Sun B, Liu Y, Yang A and Wang X 2018 Effects of oxygen concentration on helium-oxygen dielectric barrier discharges: From multi-breakdowns to single-breakdown per half-cycle *Phys. Plasmas* **25** 103511

[26] Fiebrandt M, Lackmann J W and Stapelmann K 2018 From patent to product? 50 years of low-pressure plasma sterilization *Plasma Process. Polym.* **15** 1800139

[27] Bera K, Rauf S and Collins K 2011 Plasma dynamics in low-pressure capacitively coupled oxygen plasma using PIC–MCC/fluid hybrid model *IEEE Trans. Plasma Sci.* **39** 2576–7

[28] Sharma S, Cruden B, Rao M and Bolshakov A 2004 Analysis of emission data from O_2 plasmas used for microbe sterilization *J. Appl. Phys.* **95** 3324–33

[29] Druyvesteyn M J 1930 Der niedervoltbogen *Z. Phys.* **64** 781–98

[30] Godyak V and Alexandrovich B 2015 Comparative analyses of plasma probe diagnostics techniques *J. Appl. Phys.* **118** 233302

[31] Park H and Choe W 2010 Parametric study on excitation temperature and electron temperature in low pressure plasmas *Curr. Appl. Phys.* **10** 1456–60

[32] Griem H R 1963 Validity of local thermal equilibrium in plasma spectroscopy *Phys. Rev.* **131** 1170

[33] Foissac C, Dupret C and Supiot P 2008 Electrical and spectroscopic characterizations of a low pressure argon discharge created by a broad-band helical coupling device *J. Phys. D: Appl. Phys.* **42** 015206

[34] Moon S Y, Choe W, Uhm H S, Hwang Y and Choi J 2002 Characteristics of an atmospheric microwave-induced plasma generated in ambient air by an argon discharge excited in an open-ended dielectric discharge tube *Phys. Plasmas* **9** 4045–51

[35] https://doi.org/10.18434/T4W30F

[36] Coburn J and Chen M 1980 Optical emission spectroscopy of reactive plasmas: a method for correlating emission intensities to reactive particle density *J. Appl. Phys.* **51** 3134–6

[37] Pagnon D, Amorim J, Nahorny J, Touzeau M and Vialle M 1995 On the use of actinometry to measure the dissociation in O_2 DC glow discharges: determination of the wall recombination probability *J. Phys. D: Appl. Phys.* **28** 1856

[38] Hagelaar G J M and Pitchford L C 2005 Solving the Boltzmann equation to obtain electron transport coefficients and rate coefficients for fluid models *Plasma Sources Sci. Technol.* **14** 722

[39] Niemi K, Reuter S, Graham L, Waskoenig J, Knake N, Schulz-Von Der Gathen V and Gans T 2010 Diagnostic based modelling of radio-frequency driven atmospheric pressure plasmas *J. Phys. D: Appl. Phys.* **43** 124006

[40] Kitajima T, Nakashima J, Nakano T and Makabe T 2006 Oxygen atom density in rare gas diluted O_2 radio frequency plasma *Thin Solid Films* **506** 489–93

[41] Laporta V, Celiberto R and Tennyson J 2015 Dissociative electron attachment and electron-impact resonant dissociation of vibrationally excited O_2 molecules *Phys. Rev. A* **91** 012701

[42] Aleksandrov N and Anokhin E 2009 Low-energy electron attachment and detachment in vibrationally excited oxygen *J. Phys. D: Appl. Phys.* **42** 225210

[43] Kechkar S, Swift P, Kelly S, Kumar S, Daniels S and Turner M 2017 Investigation of the electron kinetics in O_2 capacitively coupled plasma with the use of a Langmuir probe *Plasma Sources Sci. Technol.* **26** 065009

[44] Kechkar S 2015 *Experimental Investigation of a Low Pressure Capacitively-Coupled Discharge* (Dublin, Ireland: Dublin City University) Phd Thesis

[45] Godyak V, Piejak R and Alexandrovich B 1992 Measurement of electron energy distribution in low-pressure RF discharges *Plasma Sources Sci. Technol.* **1** 36

[46] Capitelli M, Colonna G, De Pascale O, Gorse C, Hassouni K and Longo S 2008 Electron energy distribution functions and second kind collisions *Plasma Sources Sci. Technol.* **18** 014014

[47] Amorim J, Lino J d S, Loureiro J, Lima M A and da Paixão F J 1999 Superelastic collisions of electrons with the c $3\Pi u$ metastable state in hydrogen dc positive column *Chem. Phys.* **246** 275–82